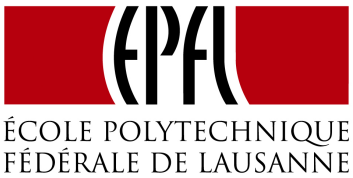

Semester Project I

Background cancellation methods

Author
Damien Maillard

Supervisor
Prof. Luis Guillermo
Villanueva

Master in Microengineering

Micro- and Nanosystems

Advanced NEMS group / LMIS1

Semester I

January 16, 2015

Contents

1 Introduction

NEMS (Nanoelectromechanical Devices) have been of particular interest in recent years due to a growing set of new applications they offer in domains such as sensitive charge detection [1], mass sensing [2] and biological imaging [3]. Their size, being reduced down to the nanometer-scale, allows high operating frequencies. Applications in the Gigahertz range have been demonstrated [4]. With devices operating faster the sensitivity is improved. As an example, a sensitivity of $12\,zN/\sqrt{Hz}$ ($1\,zN = 10^{-21}\,N$) has been achieved using a carbon nanotube resonator [5]. Moreover, NEMS have very low operating power and high quality factors [6].

2 Objectives

As the frequency increases, some issues arise in the detection of the signal coming from the device. In the example of resonators, on which this work is mainly based, it becomes more difficult to have a precise image of the resonance curve and the location of its peak (i.e. the resonance frequency) becomes problematic. The mode in which the resonator usually functions uses the properties of the resonance frequency in order to detect a change in parameter. In the case of a force sensor, the resonance frequency of the resonator undergoes a shift due to stiffness variation. Monitoring that shift allows a precise description of the applied force. It is therefore critical to obtain a precise frequency response.
In the case of NEMS, the background signal, arising from parasitic effects, can become overwhelming, completely drowning the signal of motion detection. Figure 1 shows the example of a resonance curve where the peak of resonance is embedded, and hidden, in the background. Moreover, standard measurement equipments are the cause of trouble when coming to the detection of the NEMS resonance. As an example, typical coaxial cables have intrinsic capacitances ranging from $53\,pF/m$ to $100\,pF/m$ [7]. Connecting such elements at the NEMS output acts as a low-pass filter. Therefore, the detection of resonance peaks at high frequencies becomes problematic.
The objective of this project is to explore a new background cancellation technique based on resonance frequency modulation. In order to achieve this goal, a critical review of state of the art methods has been conducted beforehand.

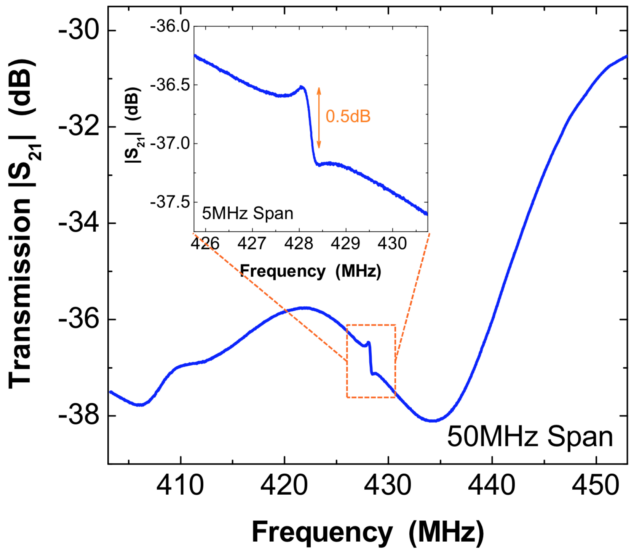

Figure 1: Resonance curve embedded in background [6]

3 Existing cancellation methods

In this section, we present diverse state of the art methods that one can use to reduce the background.

3.1 Bridging

This method was presented by the California Institute of Technology and published in *Nature Nanotechnology* in 2008 [6].
The implemented electronic circuit is shown in Figure 2. An alternative signal at Ultra high frequency[1] is sent through a power splitter. In the higher branch, the signal is not modified, whereas in the lower branch, its phase is retarded. The currents in the two branches are flowing in opposite directions. Therefore the parasitic currents arising from the presence of the NEMS resonance in the higher branch can be partially absorbed through the lower branch of the system and do not degrade the output signal. For better performance, R_B should be as close as possible to R_{DC}. Figure 3 shows the results obtained with the bridging method, along with the results obtained with standard measurement equipment, as in [8].

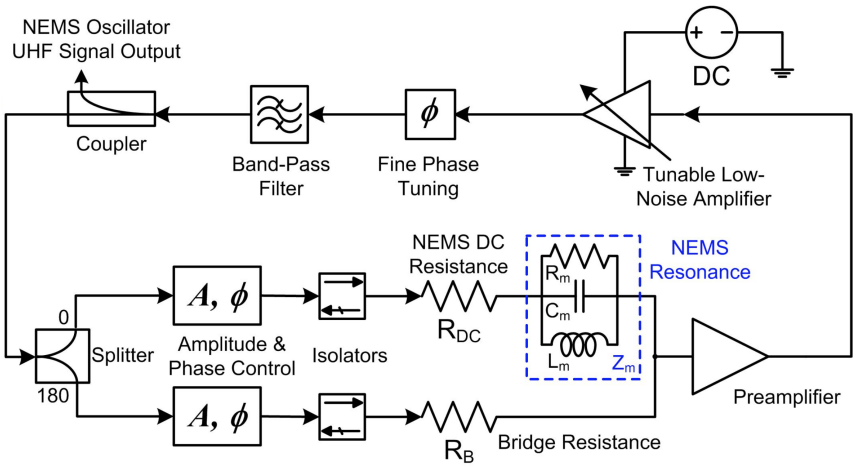

Figure 2: Electronic circuit of the bridging method

[1] between 300 MHz and 3 GHz

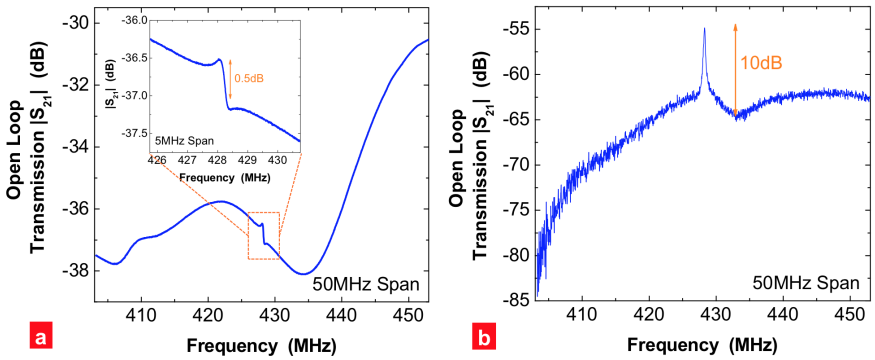

Figure 3: Results obtained (a) with the measurement equipment from [8] and (b) with the bridging method

3.2 Piezoresistive signal downmixing

This method was developed by the Condensed Matter Physics group at the California Institute of Technology and published in *Applied Physics Letters* in 2005 [9].

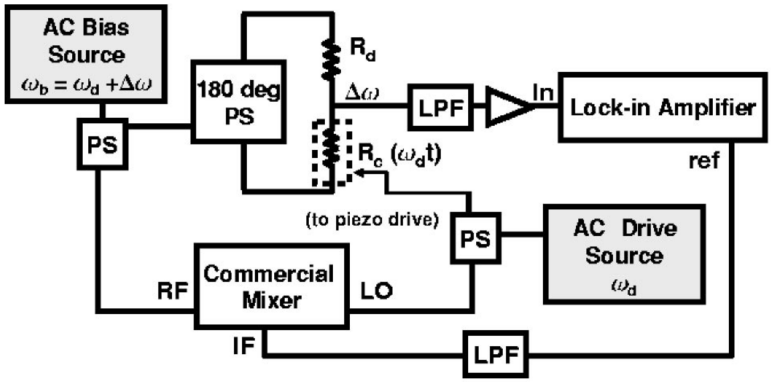

Figure 4: Set-up of the piezoresistive signal downmixing method

The set-up is depicted in Figure 4. There are two sources of alternative voltage. The first source, labelled *AC Drive Source*, is responsible for the motion of the chip. The chip consists of one piezoresistive resonator, $R_c(\omega_d\, t)$ and one dummy resistor R_d whose resistance is as close as possible to the piezoresistive resonator at rest. Figure 5 shows an optical micrograph of the cantilever along with the dummy resistor. When the chip is piezoelectrically actuated, the resonator enters in vibration and its resistance varies following an harmonic function of the drive frequency ω_d. The second voltage source, *AC Bias Source*, operating at frequency ω_b is fed to both the resonator and the dummy resistance, with a 180° phase-shift between them. The bias is therefore cancelled at the bridge point. The configuration is somehow similar to that of classic bridging.

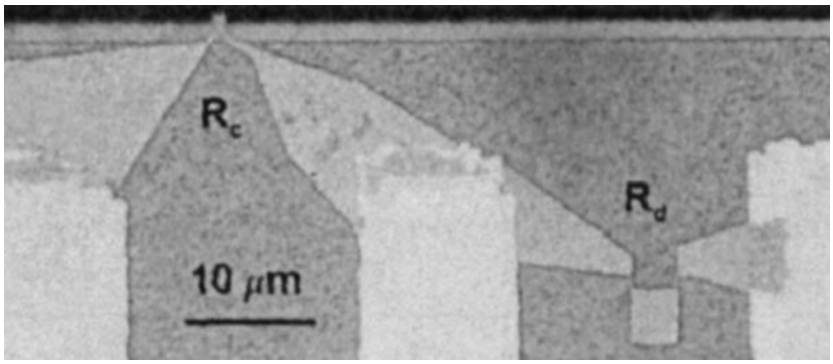

Figure 5: Optical micrograph of the actuated chip

A mixing occurs between the current flowing, at ω_b, and the resistance of the resonator, modulated at ω_d. The multiplication of signals with two different frequencies yields a signal at two frequencies, one with the addition and the other the subtraction of the frequencies. The derivation of the voltage at the output of the chip, where the branches of the resonator and the dummy resistance meet, gives us :

$$V_{out} \approx \frac{\Delta R}{4R} V_b \left[cos(\Delta\omega\, t - \phi) + cos((2\omega_d + \Delta\omega)\, t + \phi)\right] \tag{1}$$

$$\text{where } \omega_b = \omega_d + \Delta\omega$$

A complete description of the calculations can be found in Appendix A.
The low-pass filter at the input of the lock-in amplifier allows to get rid of the high frequency $2\omega_d + \Delta\omega$ term, which is of no utility because of it is strongly attenuated. The focus of our interest lies on the low-frequency term, modulated at $\Delta\omega$. Choosing $\Delta\omega$ sufficiently small (typically $<$ 100 kHz) leads to minimal attenuation by the circuitry. Moreover, the mixing occurring between the current and the piezoresistive resonator reduces the background. Our signal is finally amplified and fed to a lock-in amplifier for detection. The reference of the lock-in is generated by a commercial mixer whose inputs are the bias and the drive sources.
Figure 6 shows the results obtained for a 110-nm thick, 700-nm wide and 1.7-μm long cantilever with $V_{b0} = 1.5$ V and $\Delta\omega/2\pi = 100$ kHz, along with the results measured with a simple network analyzer.

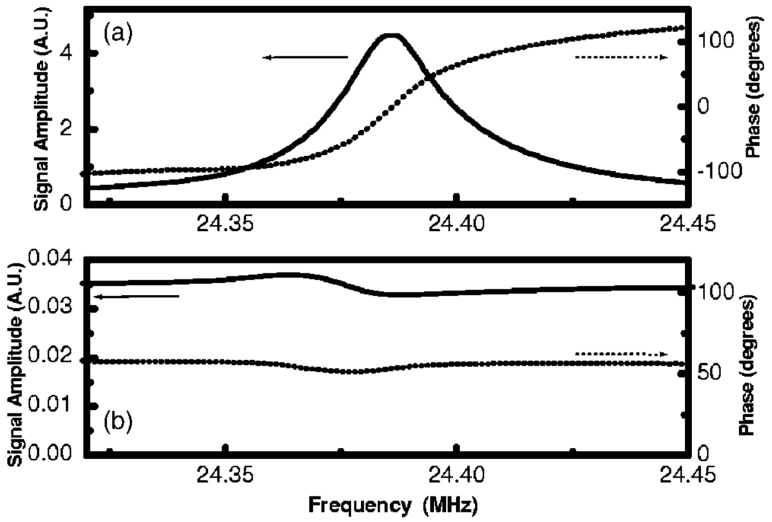

Figure 6: Signal amplitude (-) and phase (¨) of resonance of first vibration mode of 1.7-μm-long cantilever using (a) downmixing with $\Delta\omega/2\pi = 100$ kHz and (b) a network analyzer

3.3 Tunable carbon nanotube electromechanical oscillator

This method was developed by the Laboratory of Atomic and Solid-State Physics from Cornell University and published in *Nature* in 2004 [10].
Due to their nanometer-scale size, as well as outstanding electrical and mechanical properties, carbon nanotubes are excellent candidates for oscillating elements for NEMS which are operating in the MHz and GHz range [11].
The device consists of nanotubes (single- or few-walled, with diameter ranging from 1 to 4 nm) suspended over a 1.2-1.5 μm-wide, 500 nm-deep trench. An SEM image, along with the device geometry, are shown in Figure 7.

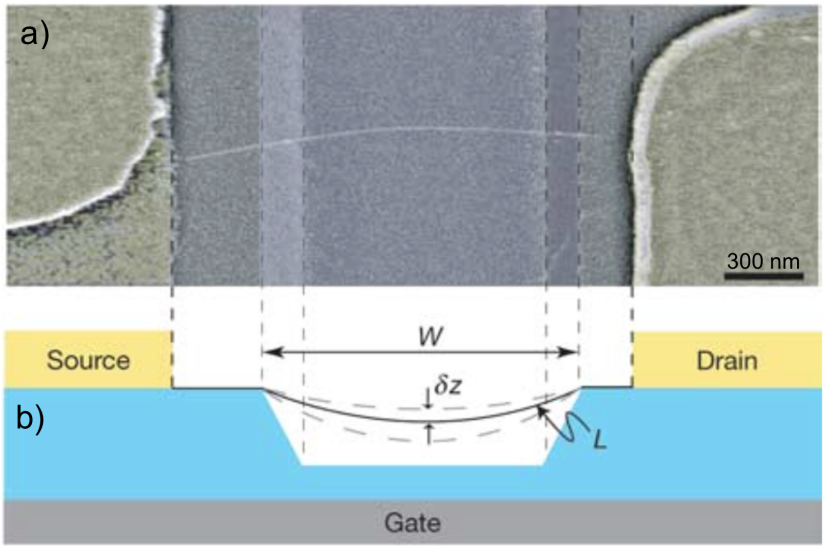

Figure 7: (a) SEM image of a suspended carbon nanotube and (b) Schematic of the device geometry

The device is actuated by electrostatic interaction between the carbon nanotube (CNT) and the gate electrode. The gate voltage is composed of a DC and an AC component, much smaller in amplitude : $V_g = V_g^{DC} + \delta V_g$. The presence of the gate voltage induces a charge on the CNT given by $q = V_g C_g$, with C_g the capacitance between the nanotube and the gate electrode. That additional charge is responsible for the actuation of the device, as it causes a force on the nanotube due to its attraction to the opposite charge $-q$, located on the gate.

The energy stored in the system is expressed as

$$W = \frac{QV}{2} = \frac{qV_g}{2} = \frac{1}{2} C_g V_g^2$$

Since the electrostatic force is conservative [12], the actuation force is the derivative of the potential energy with respect to the nanotube position. Considering

the voltage is spatially invariant :

$$F = -\frac{dW}{dz} = -\frac{1}{2}\frac{dC_g}{dz}V_g^2 = -\frac{1}{2}\frac{dC_g}{dz}((V_g^{DC})^2 + 2V_g^{DC}\delta V_g + \delta V_g^2)$$

Since the amplitude of the AC component is much smaller than the DC component, it is possible to neglect the AC square term. The electrostatic force becomes :

$$F_{el} \approx \frac{1}{2}C_g' V_g^{DC}(V_g^{DC} + 2\delta V_g) \tag{2}$$

The static component V_g^{DC} of the gate voltage controls the tension of the nanotube, and the alternative component δV_g exerts a periodic force, setting it into motion. As the frequency of the AC component becomes close to the resonance frequency of the nanotube, the displacement becomes larger and the resonator enters into resonance. The transistor properties of the nanotube tell us that the conductance change δG depends on the modulation of the induced charge q [13],[14],[15]. The variation of the induced charge (assumed small) can be expressed as :

$$\delta q = \delta(C_g V_g) = C_g \delta V_g + V_g \delta C_g \tag{3}$$

The first term of equation (3), the modulation of the charge due to the modulation of the gate voltage, occurs at the driving frequency ω. The second term, due to the modulation of the capacitance between the nanotube and the gate, exists only if the tube is moving. In our case, the motion occurs at the driving frequency as well, so the modulation of the charge, and therefore the total modulation of the conductance are only happening at ω.

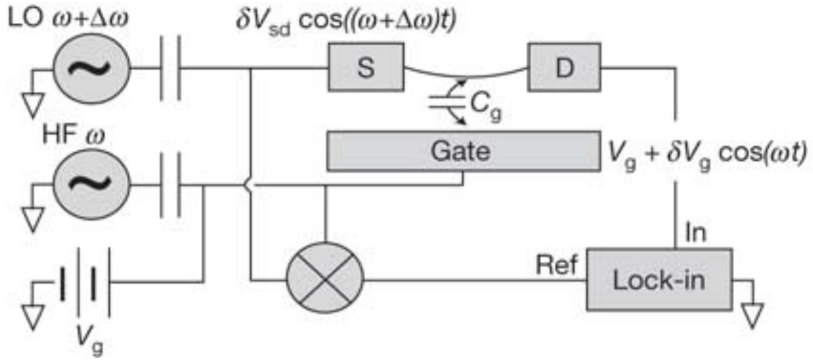

Figure 8: Set-up of the system used to detect the motion of the carbon nanotube

The setup of the system is shown in Figure 8. The current flowing through the CNT, detected by the lock-in amplifier, is expressed as the product of the

voltage on the source electrode with the conductance of the nanotube :

$$I = GV_{sd} = G^{DC}V_{sd}^{DC} + G^{DC}\delta V_{sd}^{AC} + \delta G^{AC}V_{sd}^{DC} + \underbrace{\delta G^{AC}\delta V_{sd}^{AC}}_{\delta I^{lock-in}} \qquad (4)$$

The first two terms of equation (4) are not consequences of the motion of the nanotube (they are proportional to G^{DC}) and are not relevant in our analysis. The third term is occurring at the frequency ω and will be hidden by the background due to the motion of the nanotube. The term of interest is the last : the mixing between the modulated conductance δG (at ω) and the source-drain voltage (at $\omega + \Delta\omega$) gives the low frequency component detected by the lock-in amplifier.

The calculations made in [16] give :

$$\delta I^{lock-in} = \delta G\, \delta V_{sd} = \frac{1}{2\sqrt{2}} \frac{dG}{dV_g} \left(\delta V_g + V_g^{DC} \frac{\delta C_g}{C_g}\right) \delta V_{sd} \qquad (5)$$

In equation (5), we notice that the conductance is somehow proportional to het induced charge from equation (3). The results obtained with the method are shown in figure 9. We see a distinctive feature, attributed to the resonance motion of the nanotube (which modulates the capacitance), on top of a slowly changing background due to the actuating gate voltage.

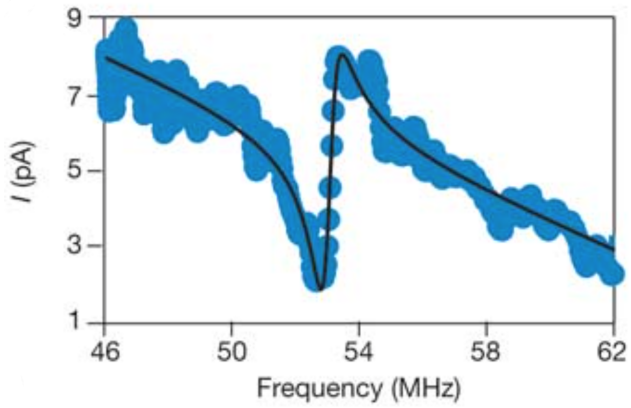

Figure 9: Measured current as function of the driving frequency

It is possible to improve the results using the same device and an identical detection method. The difference lies in the actuation : if the gate voltage is purely alternative, the modulation of the capacitance does not occur at the same frequency as the gate voltage. Indeed, since the force is proportional to the square of the gate voltage, we have :

$$F \propto V_g^2 = (V_g^{AC})^2 = (V_g\, cos(\frac{\omega}{2}\, t))^2 = V_g^2\, cos^2(\frac{\omega}{2}\, t) = \frac{1}{2}\, V_g^2 + \frac{1}{2}\, V_g^2\, cos(\omega\, t)$$

We notice that the force has a static component, as well as an alternative component at twice the frequency of actuation. In this case, the modulation of the capacitance occurs at the frequency ω whereas the modulation of the gate voltage occurs at the frequency $\frac{\omega}{2}$. The modulation of the conductance is therefore splitted into two different frequencies. The mixing of the conductance with the source-drain voltage gives signals at four different frequencies.
Mathematically :

$$\begin{aligned}\delta I^{lock-in} &\propto [cos(\frac{\omega}{2}\, t) + cos(\omega\, t)]\, cos((\omega + \Delta\omega)\, t) \\ &= cos((\frac{3\,\omega}{2} + \Delta\omega)\, t) + cos((\frac{\omega}{2} + \Delta\omega)\, t) + cos((2\,\omega + \Delta\omega)\, t) + cos(\Delta\omega\, t)\end{aligned} \tag{6}$$

In equation (6), the low-frequency term of interest (at $\Delta\omega$) is only due to the mixing of the capacitance modulation. The modulation of the gate voltage creates terms at other frequencies. This splitting of the effects allows for a reduction of the background, because the term that the lock-in amplifier detects is now only dependent on the motion, and is not function of the gate voltage anymore.

The diagrams in Figure 10 sum up the differences between the two methods presented in this section.

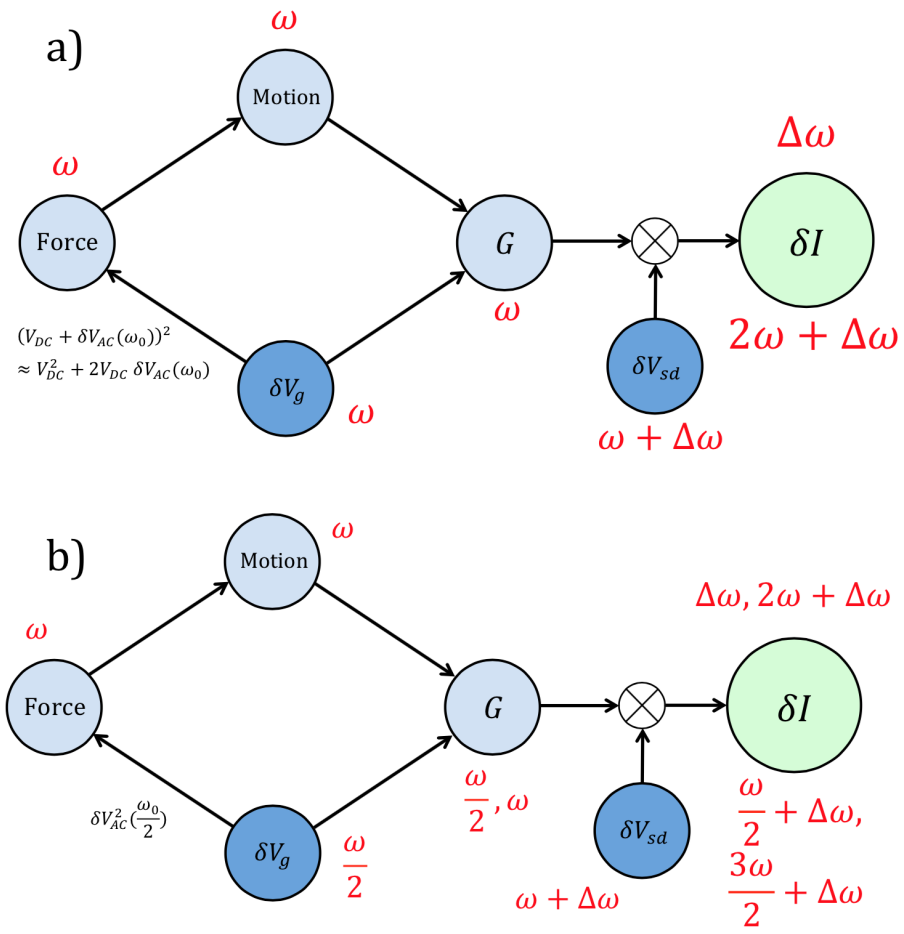

Figure 10: Scheme of the frequencies involved in the two methods (a) Motion linearly proportional to the AC gate voltage (detection modulation) and (b) Motion proportional to the square of the AC gate voltage (actuation and detection modulation)

3.4 FM Demodulation of a Doubly Clamped Carbon Nanotube Oscillator

The work presented in this section was achieved by the Laboratoire de Physique de la Matière Condensée et Nanostructures at Lyon University and published in *Small* in 2010 [17].
The setup of the system is pictured in Figure 11. The lock-in amplifier sends a low-frequency reference signal at ω_L to the input of a radio frequency generator. The output of the generator is a frequency modulated signal expressed as :

$$V^{FM}(t) = V_c\, cos(\Psi(t)) \text{ with } \Psi(t) = \omega_c\, t + \frac{\omega_\Delta}{\omega_L}\, sin(\omega_L\, t) \tag{7}$$

where V_c is the applied voltage,
ω_c the carrier frequency,
ω_Δ the frequency deviation,
t the time.

That signal is then applied to the source electrode of a carbon nanotube and is responsible for the motion of the nanotube. The gate voltage is static.

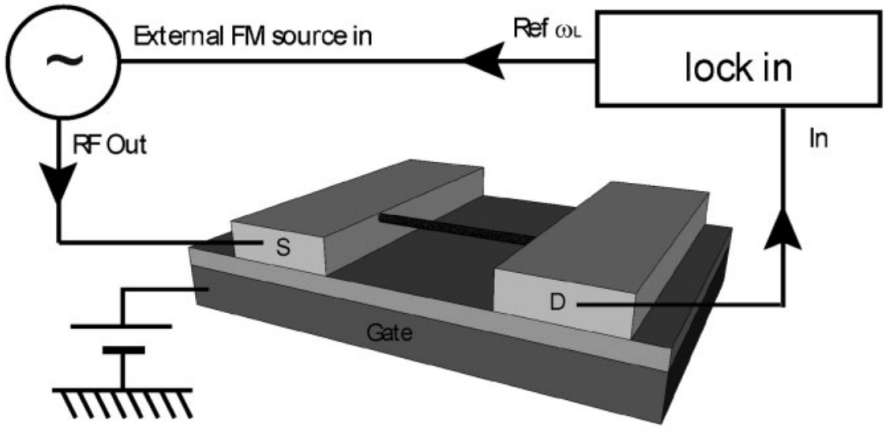

Figure 11: Setup of the system for the Frequency Modulation method

The source-drain current $I_{sd}(t)$, flowing through the nanotube, depends on three parameters :

- the voltage V_{sd}
- the position $x(t)$ of the middle of the nanotube
- the gate voltage V_g

A Taylor expansion of $I_{sd}(t)$ around $V_{sd} = 0$, $x(t) = x_0$, $V_g = V_g^{DC}$ yields :

$$I(V(t), x_0 + \delta x(t), V_g^{DC}) = \underbrace{I(0, x_0, V_g^{DC})}_{\substack{=0 \\ \text{no current flowing if} \\ \text{no source-drain voltage}}} + \underbrace{\frac{\partial I}{\partial V_{sd}}(0, x_0, V_g^{DC})V(t)}_{\substack{\neq 0, \text{ at high carrier frequency} \\ \text{not of interest}}} + \underbrace{\frac{\partial I}{\partial x}(0, x_0, V_g^{DC})}_{\substack{=0 \\ \text{no source-drain} \\ \text{voltage}}} \delta x(t) + \underbrace{\frac{\partial I}{\partial V_g}(0, x_0, V_g^{DC})}_{\substack{=0 \\ V_g = \text{const}}} V_g^{DC} + I_2 \quad (8)$$

In the equation above, the term I_2 represents the higher terms of the expansion. Considering that $\frac{\partial I}{\partial V_g^{DC}} = 0$, the second order of the Taylor expansion gives :

$$I_2(V(t), x_0 + \delta x(t), V_g^{DC}) = \frac{1}{2}\frac{\partial^2 I}{\partial V_{sd}^2}(0, x_0, V_g^{DC})(V(t))^2 + \frac{\partial^2 I}{\partial V_{sd}\partial x}(0, x_0, V_g^{DC})V(t)\delta x(t) + \frac{1}{2}\underbrace{\frac{\partial^2 I}{\partial x^2}(0, x_0, V_g^{DC})}_{\substack{=0 \\ \text{no source-drain} \\ \text{voltage}}}(\delta x(t))^2 + I_3 \quad (9)$$

The first term of equation (9) has no signal at the modulation frequency ω_L. The complete development of that statement can be found in Appendix B.

The remaining term is the electromechanical current. It is possible to rewrite the argument of the cosine in the $V^{FM}(t)$ signal from equation (7) :

$$\Psi(t + \Delta t) = \Psi(t) + \frac{\partial \psi}{\partial t}\Delta t \quad (10)$$

Here Δt represents a time smaller than the timescale of the oscillator, i.e. $\Delta t < Q/\omega_0$, where Q is the quality factor and ω_0 the resonance frequency of the resonator. We consider that the modulation ω_L is happening too slowly for the resonator, oscillating near ω_0, to detect it. There are some conditions to be met : $\omega_c >> \omega_\Delta$, $\omega_0/Q >> \omega_L$. Moreover, with the electromechanical current is only significant at the resonance frequency, the carrier frequency must be close to the resonance frequency : $\omega_c \approx \omega_0$. It is therefore possible to consider that the nanotube is submitted at each time t to a harmonic forcing at the instantaneous frequency, i.e. $\omega_i = \partial\Psi/\partial t = \omega_c + \omega_\Delta\, cos(\omega_L\, t)$ with an additional phase term $\Psi(t)$ constant over the timescale of interest.

The electromechanical current can be rewritten as :

$$I^{FM} = \frac{\partial^2 I}{\partial x \partial V_{sd}}\, V_c\, cos(\omega_i\, \Delta t + \Psi(t))\, \delta x(t + \Delta t) \quad (11)$$

Calculations for the last term to be determined give :

$$\delta x(t+\Delta t) = \mathrm{Re}\{\delta x * (\omega_i)\}\, cos(\omega_i\, \Delta t + \Psi(t)) - \mathrm{Im}\{\delta x * (\omega_i)\}\, sin(\omega_i\, \Delta t + \Psi(t)) \tag{12}$$

The development of that last result can be found in Appendix B.
Injecting the equation (12) into (11) :

$$\begin{aligned} I^{FM} &= \frac{\partial^2 I}{\partial x \partial V_{sd}}\, V_c\, cos(\omega_i\, \Delta t + \Psi(t))\, [\mathrm{Re}\{\delta x * (\omega_i)\}\, cos(\omega_i\, \Delta t + \Psi(t)) \\ &\qquad - \mathrm{Im}\{\delta x * (\omega_i)\}\, sin(\omega_i\, \Delta t + \Psi(t))] \\ &= \frac{\partial^2 I}{\partial x \partial V_{sd}}\, V_c\, [\mathrm{Re}\{\delta x * (\omega_i)\}\, cos^2(\omega_i\, \Delta t + \Psi(t)) \\ &\qquad - \mathrm{Im}\{\delta x * (\omega_i)\}\, cos(\omega_i\, \Delta t + \Psi(t))\, sin(\omega_i\, \Delta t + \Psi(t))] \\ &= \frac{\partial^2 I}{\partial x \partial V_{sd}}\, V_c\, [\mathrm{Re}\{\delta x * (\omega_i)\}\, (\frac{1}{2} + \frac{1}{2}\, cos(2\, \omega_i\, \Delta t + 2\, \Psi(t))) \\ &\qquad - \mathrm{Im}\{\delta x * (\omega_i)\}\, \frac{1}{2}\, sin(2\, \omega_i\, \Delta t + 2\, \Psi(t))] \end{aligned} \tag{13}$$

From equation (13), the low-frequency term of the electromechanical current is extracted :

$$I_{LF}^{FM} = \frac{1}{2}\, \frac{\partial^2 I}{\partial x \partial V_{sd}}\, V_c\, \mathrm{Re}\{\delta x * (\omega_i)\} \tag{14}$$

Finally, a Taylor expansion of $\mathrm{Re}\{\delta x * (\omega_i)\}$, with $\omega_\Delta << \omega_c$, gives :

$$\begin{aligned} \mathrm{Re}\{\delta x * (\omega_i)\} &= \mathrm{Re}\{\delta x * (\omega_c)\} + \frac{\partial \mathrm{Re}\{\delta x *\}}{\partial \omega_i}\, \omega_\Delta\, cos(\omega_L\, t) \\ &\quad + \frac{1}{2}\, \frac{\partial^2 \mathrm{Re}\{\delta x *\}}{\partial \omega_i^2}\, \omega_\Delta^2\, cos^2(\omega_L\, t) + ... \end{aligned} \tag{15}$$

We notice that there is no term in $sin(\omega_L\, t)$ and no purely electrical term in $cos(\omega_L\, t)$. Therefore, there is no additional background, because the detected current at ω_L is purely electromechanical.

Figure 12 shows the results obtained. The curve obtained is indeed the derivative of the real part of the Lorentzian. The Appendix B contains a qualitative verification of that statement.

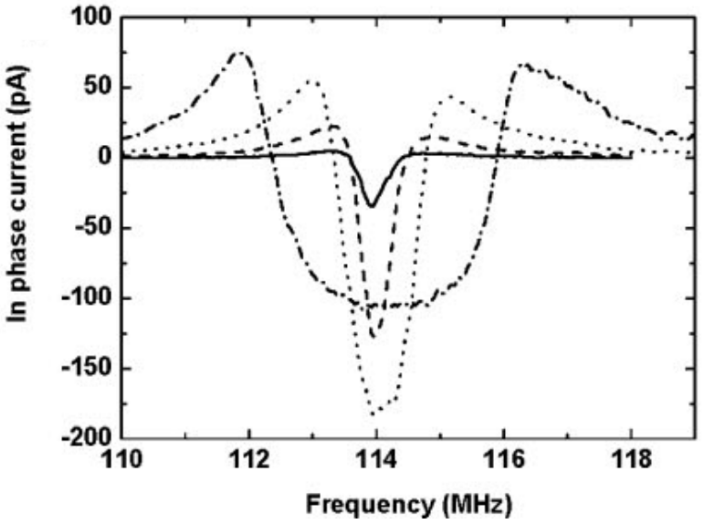

Figure 12: Current amplitude versus carrier frequency ω_c for $\omega_\Delta/2\pi$=50 kHz (solid line), $\omega_\Delta/2\pi$=200 kHz (dashed line), $\omega_\Delta/2\pi$=700 kHz (dotted line) and $\omega_\Delta/2\pi$=2 MHz (dashed dotted line)

4 New method developed : modulation of the resonance frequency

In the Frequency Modulation method, the actuation was modulated around the carrier frequency ω_c, and the carbon nanotube had a constant stiffness and therefore a constant resonance frequency. In this new method we developed, the actuation force is constant and we change the stiffness of the resonator by piezoelectric tuning. The resonance frequency of the resonator is modulated, and mixing occurs between the motion of the beam and the shifting Lorentzian curve. Figure 13 depicts the fondamental difference between the FM method and the new method developed.

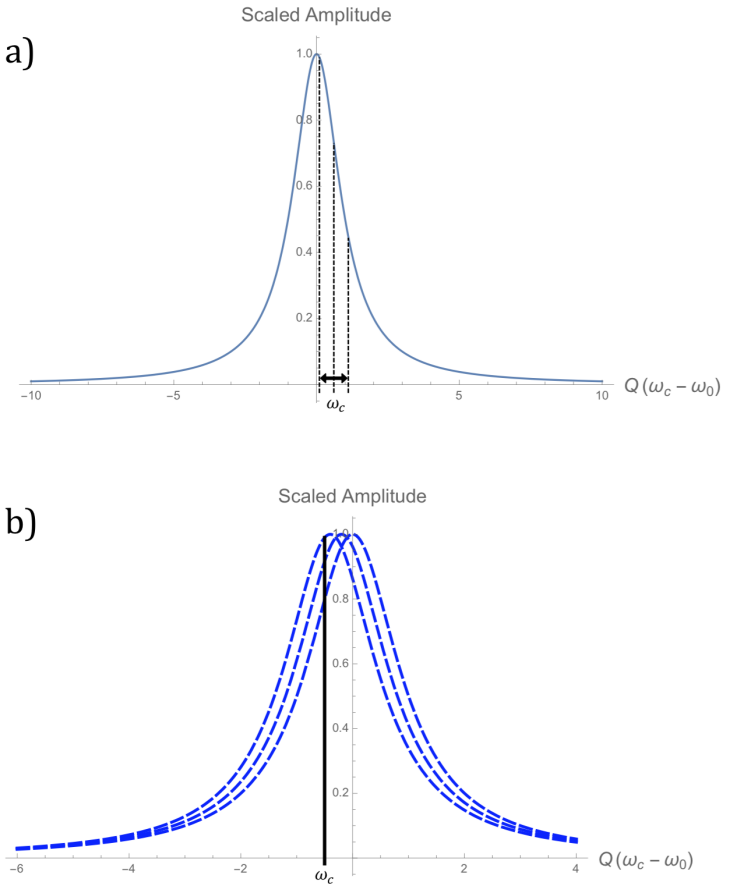

Figure 13: a) FM : the actuation force is modulated and the resonance frequency peak is fixed. b) New method : the actuation force is fixed and the resonance curve of the resonator is modulated.

4.1 Calculations

We consider the following equation of motion :

$$\ddot{x}(t) + \frac{1}{Q}\,\omega_R(t)\,\dot{x}(t) + \omega_R^2(t)\,x(t) = F_{act} \tag{16}$$

with an actuation force at constant frequency ω_c

$$F_{act} = F_0\,cos(\omega_c\,t + \phi)$$

or in complex notation

$$F_{act} = F_0\,e^{j\,\omega_c\,t} \tag{17}$$

Due to the piezoelectric tuning of the resonator, the resonance frequency $\omega_R(t)$ is modulated at ω_L :

$$\omega_R(\omega_0, \omega_L, \Delta\omega, t) = \omega_0 + \Delta\omega\,cos(\omega_L\,t)$$

or in complex notation

$$\omega_R(\omega_0, \omega_L, \Delta\omega, t) = \omega_0 + \frac{1}{2}\,\Delta\omega\,e^{-j\,\omega_L\,t} + \frac{1}{2}\,\Delta\omega\,e^{j\,\omega_L\,t} \tag{18}$$

We assume that the motion is happening at three frequencies : the resonance frequency, and frequencies depending on the modulation ω_L. Assuming complex amplitudes, it is possible to take an actuation force F_0 that is real because the phase changes will be related to the imaginary parts of the amplitude coefficients. The motion is assumed to be :

$$x(t) = A\,e^{j\,\omega_c\,t} + B_1\,e^{j\,(\omega_c+\omega_L)\,t} + B_2\,e^{j\,(\omega_c-\omega_L)\,t} \tag{19}$$

Inserting equations (17), (18) and (19) along with its first and second derivatives into equation (16), and neglecting the terms in the second order of $\Delta\omega$ (because $\Delta\omega << \omega_0$), we get terms at five different frequencies. Three of those frequencies are indeed coming from the motion that we have assumed (ω_c, $\omega_c+\omega_L$, $\omega_c-\omega_L$). The last two frequencies of the signal are $\omega_c + 2\,\omega_L$ and $\omega_c - 2\,\omega_L$, which can be neglected because their amplitude is negligible.
Taking only the terms at the frequencies of interest and assuming the amplitude to be complex, it is possible to express the equation of motion with the terms sorted according to their frequencies. Redefinition of the parameters, as well as assumptions, have to be made in order to continue with the analysis :

$$\begin{aligned}
&\Delta\omega = \gamma\,\omega_0 \\
&\omega_L = \delta\,\omega_0 \\
&\omega_c = \omega_0\,(1 + \frac{\chi}{Q})
\end{aligned}$$

Assumptions :

$$\delta,\ \gamma,\ \epsilon << 1$$

Those assumptions allow us to greatly simplify the calculations. Sorting the terms according to their frequencies, and splitting the real and imaginary parts, we obtain six equations with six unknown variables :

$$\begin{cases} \dfrac{(-A_{im} + B_{1,re}\,Q\,\gamma + B_{2,re}\,Q\,\gamma - 2\,A_{re}\,\chi)\,\omega_0^2}{Q}\,e^{j\,\omega_c\,t} = F_0\,e^{j\,\omega_c\,t} \\ \dfrac{(A_{re} + B_{1,im}\,Q\,\gamma + B_{2,im}\,Q\,\gamma - 2\,A_{im}\,\chi)\,\omega_0^2}{Q}\,e^{j\,\omega_c\,t} = 0 \\ \dfrac{(-B_{1,im} + A_{re}\,Q\,\gamma - 2\,B_{1,re}\,\chi)\,\omega_0^2}{Q}\,e^{j\,(\omega_c+\omega_L)\,t} = 0 \\ \dfrac{(B_{1,re} + A_{im}\,Q\,\gamma - 2\,B_{1,im}\,\chi)\,\omega_0^2}{Q}\,e^{j\,(\omega_c+\omega_L)\,t} = 0 \\ \dfrac{(-B_{2,im} + A_{re}\,Q\,\gamma - 2\,B_{2,re}\,\chi)\,\omega_0^2)}{Q}\,e^{j\,(\omega_c-\omega_L)\,t} = 0 \\ \dfrac{(B_{2,re} + A_{im}\,Q\,\gamma - 2\,B_{2,im}\,\chi)\,\omega_0^2}{Q}\,e^{j\,(\omega_c-\omega_L)\,t} = 0 \end{cases}$$

Solving with Mathematica, and adding the assumption that $\delta,\ \gamma << \epsilon$ we get the following results :

$$\begin{cases} A_{re} = -\dfrac{2\,F_0\,Q\,\chi}{(1+4\,\chi^2)\,\omega_0^2} \\ A_{im} = -\dfrac{F_0\,Q}{(1+4\,\chi^2)\,\omega_0^2} \\ B_{1,re} = -\dfrac{F_0\,Q^2\,\gamma(4\chi^2-1)}{(1+4\chi^2)^2\,\omega_0^2} \\ B_{1,im} = -\dfrac{4\,F_0\,Q^2\,\gamma\,\chi}{(1+4\chi^2)^2\,\omega_0^2} \\ B_{2,re} = -\dfrac{F_0\,Q^2\,\gamma(4\chi^2-1)}{(1+4\chi^2)\,\omega_0^2} \\ B_{2,im} = -\dfrac{4\,F_0\,Q^2\,\gamma\,\chi}{(1+4\chi^2)^2\,\omega_0^2} \end{cases}$$

We notice that B_1 and B_2 are identical. This is coherent, because we modulate the resonance frequency with the same amplitude on both sides of the actuation frequency. The final signal that we obtain at the output has components with four different frequencies :

- ω_c : motion and background (actuation)
- $\omega_c + \omega_L$: only motion
- $\omega_c - \omega_L$: only motion
- ω_L : background (modulation frequency, electrical tuning)

We want to observe a signal that is as free as possible from background. By multiplying the output by $cos((\omega_c + \omega_L)\,t)$, we obtain a term at DC that is

depending on the motion. This is the term of interest that we want to observe to describe the motion of the resonator.

4.2 Numerical simulations

In this section, we have set values of the quality factor at $Q = 1000$ and the amplitude ratio of the modulation to the resonance frequency at $\gamma = 10^{-}5$. Figure 14 shows the real and imaginary parts of the amplitude B_1, representing the frequency of interest $\omega_c + \omega_L$. Figure 15 shows the real parts of A and B. As expected, since most of the motion occurs at the resonance frequency $\omega_c \approx \omega_0$, A is much larger than B.

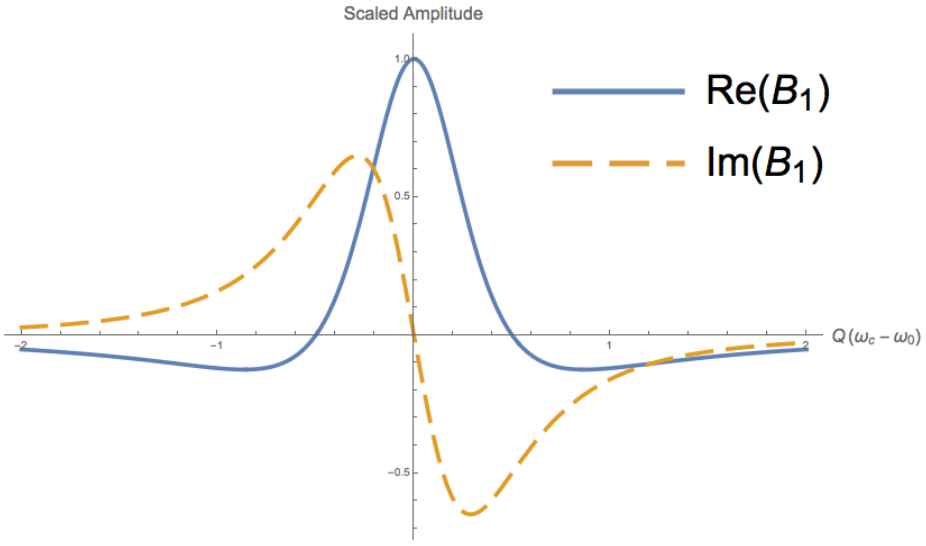

Figure 14: Scaled amplitude of the real and imaginary parts of the amplitude B_1. The x-axis represents the distance between the actuation force and the actual resonance frequency.

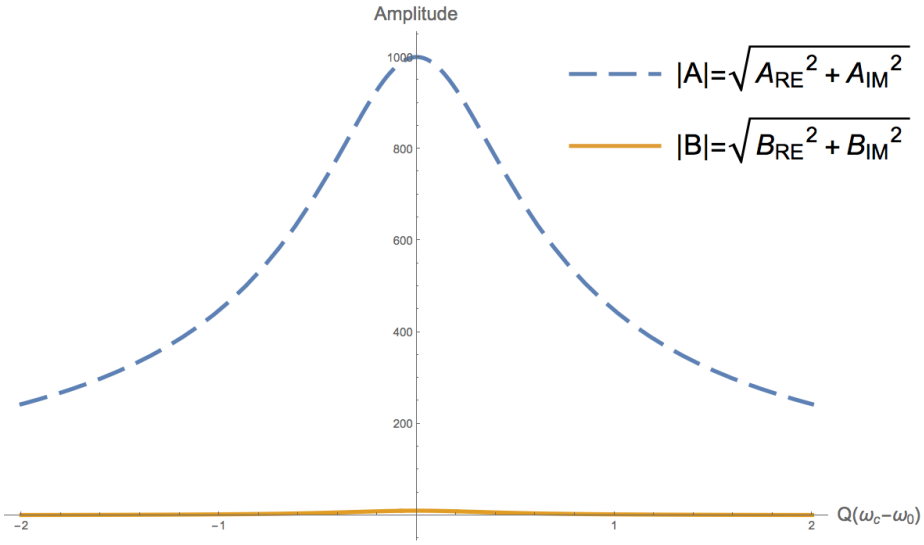

Figure 15: Amplitude of the reals parts of A and B. We notice that $|A| >> |B|$.

5 Conclusion

5.1 Summary

The presence of background signals in the frequency response of a resonator is a problematic of great importance in the domain of Nano Electromechanical Devices. The promising features offered by miniaturisation of systems come at a price : the sensitivity can be greatly improved, but the motion detection is hindered.

Different groups have been working on methods to enhance the description of the resonance curve. The progress achieved in the area of carbon nanotubes and their use as resonators allowed for efficient background reduction. In particular, the Frequency Modulation showed a detection method free of additional electrical components.

The new method developed in this project is based on the modulation of the resonance frequency, which is a property that has not been explored as a background cancellation technique so far. The theoretical analysis shows very promising results.

5.2 Outlook

The calculations, as well as some numerical simulations, were conducted for the resonance frequency modulation technique. The next step in the development of this method is to verify the fidelity of the theoretical results with experimental data. The fabrication of the devices is particularly challenging due to the small size. Therefore, state of the art clean room equipment is expected to be necessary.

A parameter that has not been taken into account in this work is the noise. As an oscillating device is reduced in size, its motion can be altered by thermal fluctuations, as well as other forms of external noise, such as 1/f. It would be interesting to study how noise affects the motion of the NEMS resonator and how the cancellation technique responds to the noise.

Acknowledgement

I would like to thank my supervisor, Prof. Luis Guillermo Villanueva. Without his patience and availability through every step of this project, I would not have been able to fully understand the complicated concepts at take in the background cancellation.
I also thank the LMIS1 and the Advanced NEMS group for granting me access to their premises.

6 References

[1] A. N. Cleland and M. L. Roukes. A nanometre-scale mechanical electrometer. *Nature*, 392(6672):160–162, 03 1998.

[2] K. L. Ekinci, X. M. H. Huang, and M. L. Roukes. Ultrasensitive nanoelectromechanical mass detection. *Applied Physics Letters*, 84(22):4469–4471, 2004.

[3] J. Sidles, J. Garbini, K. Bruland, D. Rugar, O. Züger, S. Hoen, and C. Yannoni. Magnetic resonance force microscopy. *Reviews of Modern Physics*, 67(1):249–265, 01 1995.

[4] X. M. H. Huang, C. A. Zorman, M. Mehregany, and M. L. Roukes. Nanoelectromechanical systems: Nanodevice motion at microwave frequencies. *Nature*, 421(6922):496–496, 01 2003.

[5] J. Moser, J. Guttinger, A. Eichler, M. J. Esplandiu, D. E. Liu, M. I. Dykman, and A. Bachtold. Ultrasensitive force detection with a nanotube mechanical resonator. *Nat Nano*, 8(7):493–496, 07 2013.

[6] X. L. Feng, C. J. White, A. Hajimiri, and M. L. Roukes. A self-sustaining ultrahigh-frequency nanoelectromechanical oscillator. *Nat Nano*, 3(6):342–346, 06 2008.

[7] Table 2, http://electronicdesign.com/energy/coaxial-cable-still-best-way-make-rf-connection, December 2014.

[8] X. M. H. Huang, X. L. Feng, C. A. Zorman, M. Mehregany, and M. L. Roukes. Vhf, uhf and microwave frequency nanomechanical resonators. *New J. Phys.*, 7(247), 2005.

[9] I. Bargatin, E. B. Myers, J. Arlett, B. Gudlewski, and M. L. Roukes. Sensitive detection of nanomechanical motion using piezoresistive signal downmixing. *Applied Physics Letters*, 86(133109), 2005.

[10] V. Sazonova, Y. Yaish, H. Ustunel, D. Roundy, T. A. Arias, and P. L. McEuen. A tunable carbon nanotube electromechanical oscillator. *Nature*, 431(7006):284–287, 09 2004.

[11] A. Kis and A. and Zettl. Nanomechanics of carbon nanotubes. *Philosophical Transactions of the Royal Society of London A: Mathematical, Physical and Engineering Sciences*, 366(1870):1591–1611, 05 2008.

[12] http://www.mit.edu/ jhurwitz/8.022/2010-09-20.pdf, December 2014.

[13] S. J. Tans, A. R. M. Verschueren, and C. Dekker. Room-temperature transistor based on a single carbon nanotube. *Nature*, 393(6680):49–52, 05 1998.

[14] C. Zhou, J. Kong, and H. Dai. Intrinsic electrical properties of individual single-walled carbon nanotubes with small band gaps. *Physical Review Letters*, 84(24):5604–5607, 06 2000.

[15] E. D. Minot, Y. Yaish, V. Sazonova, and P. L. McEuen. Determination of electron orbital magnetic moments in carbon nanotubes. *Nature*, 428(6982):536–539, 04 2004.

[16] V. Sazonova. *A tunable carbon nanotube resonator*. PhD thesis, Cornell University, August 2006.

[17] V. Gouttenoire, T. Barois, S. Perisanu, J.-L. Leclercq, S. T. Purcell, P. Vincent, and A. Ayari. Digital and fm demodulation of a doubly clamped single-walled carbon-nanotube oscillator: Towards a nanotube cell phone. *Small*, 6(9):1060–1065, 2010.

A Piezoresistive downmixing calculations

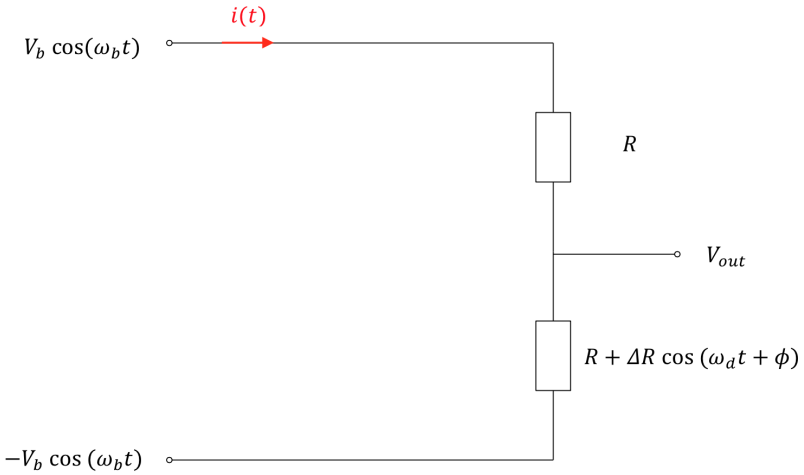

Figure 16: Electronic circuit of the piezoresistive downmixing device

Using Kirchhoff's voltage law in the circuit depicted in Figure 16, we obtain the equations :

$$-V_b\,cos(\omega_b\,t) + R\,i(t) + (R + \Delta R\,cos(\omega_d\,t + \phi))\,i(t) - V_b\,cos(\omega_b\,t) = 0 \quad \text{(A.1)}$$

$$-V_b\,cos(\omega_b\,t) + R\,i(t) + V_{out} = 0 \quad \text{(A.2)}$$

From equation (A.1) :

$$-2\,V_b\,cos(\omega_b\,t) + (2R + \Delta R\,cos(\omega_d\,t + \phi))\,i(t) = 0$$

$$i(t) = \frac{2\,V_b\,cos(\omega_d\,t)}{R\,(2 + \frac{\Delta R}{R}\,cos(\omega_d\,t + \phi))} \quad \text{(A.3)}$$

Inserting equation (A.3) into (A.2) :

$$\begin{aligned} V_{out} &= V_b\,cos(\omega_b\,t) - R\,\frac{2\,V_b\,cos(\omega_d\,t)}{R\,(2 + \frac{\Delta R}{R}\,cos(\omega_d\,t + \phi))} \\ &= \frac{\frac{\Delta R}{2R}\,cos(\omega_b\,t)\,cos(\omega_d\,t + \phi)}{1 + \frac{\Delta R}{2R}\,cos(\omega_d\,t + \phi)} \approx \frac{\Delta R}{2R}\,cos(\omega_b\,t)\,cos(\omega_d\,t + \phi) \\ &\approx \frac{\Delta R}{4R}\,V_b\,[cos((\omega_b + \omega_d)\,t + \phi) + cos((\omega_b - \omega_d)\,t - \phi)] \end{aligned}$$

Defining the low frequency $\Delta\omega = \omega_b - \omega_d$, we obtain the expression :

$$V_{out} \approx \frac{\Delta R}{4R} V_b \left[cos(\Delta\omega\, t - \phi) + cos((2\omega_d + \Delta\omega)\, t + \phi) \right] \tag{A.4}$$

B Frequency Modulation calculations

Demonstration : Absence of terms at frequency ω_L in $V(t)^2$

The frequency modulated signal, from equation (7) can be written in a different manner :

$$\begin{aligned} V(t) &= V_c\,[cos(\omega_c\,t)\,cos(\Psi(t)) - sin(\omega_c\,t)\,sin(\Psi(t))] \\ &= V_c\,[cos(\omega_c\,t)\,cos(\frac{\omega_\Delta}{\omega_L}\,sin(\omega_L\,t)) - sin(\omega_c\,t)\,sin(\frac{\omega_\Delta}{\omega_L}\,sin(\omega_L\,t))] \end{aligned} \tag{B.1}$$

The Jacobi-Anger expansion properties[2] state :

$$cos(z\,sin(\theta)) = J_0(z) + 2\sum_{n=1}^{\infty} J_{2n}(z)\,cos(2n\,\theta) \tag{B.2}$$

$$sin(z\,sin(\theta)) = 2\sum_{n=1}^{\infty} J_{2n-1}(z)\,sin((2n-1)\,\theta) \tag{B.3}$$

Substituting z by $\frac{\omega_\Delta}{\omega_L}$ and θ by $\omega_L\,t$ in (B.2) and (B.3) and injecting those equations into (B.1), we get

$$\begin{aligned} V(t) &= V_c\,\{cos(\omega_c t)\,[J_0(\frac{\omega_\Delta}{\omega_L}) + 2\sum_{n=1}^{\infty} J_{2n}(\frac{\omega_\Delta}{\omega_L})\,cos(2n\,\omega_L t)] \\ &\quad -\ sin(\omega_c t)\ *2\sum_{n=1}^{\infty} J_{2n-1}(\frac{\omega_\Delta}{\omega_L})\,sin((2n-1)\,\omega_L t)\} \\ &= V_c\,J_0(\frac{\omega_\Delta}{\omega_L})\,cos(\omega_c t) + \underbrace{2\,V_c\sum_{n=1}^{\infty} J_{2n}(\frac{\omega_\Delta}{\omega_L})\,cos(\omega_c t)\,cos(2n\,\omega_L t)}_{\text{A}} \\ &\quad \underbrace{-\ 2\,V_c\sum_{n=1}^{\infty} J_{2n-1}(\frac{\omega_\Delta}{\omega_L})\,sin(\omega_c t)\,sin(2(n-1)\,\omega_L t)}_{\text{B}} \end{aligned} \tag{B.4}$$

Splitting the equation for clarity purposes :

$$\begin{aligned} \text{A:}\ & 2\,V_c\sum_{n=1}^{\infty} J_{2n}(\frac{\omega_\Delta}{\omega_L})\,cos(\omega_c t)\,cos(2n\,\omega_L t) \\ &= 2\,V_c\sum_{n=1}^{\infty} J_{2n}(\frac{\omega_\Delta}{\omega_L})\,[\frac{1}{2}cos((\omega_c - 2n\,\omega_L)\,t) + \frac{1}{2}cos((\omega_c + 2n\,\omega_L)\,t)] \\ &= V_c\sum_{n=1}^{\infty} J_{2n}(\frac{\omega_\Delta}{\omega_L})\,[cos((\omega_c - 2n\,\omega_L)\,t) + cos((\omega_c + 2n\,\omega_L)\,t)] \end{aligned} \tag{B.5}$$

[2] http://en.wikipedia.org/wiki/Jacobi-Anger expansion

$$
\begin{aligned}
\text{B: } & 2\,V_c \sum_{n=1}^{\infty} J_{2n-1}(\frac{\omega_\Delta}{\omega_L})\, sin(\omega_c t)\, sin(2(n-1)\,\omega_L t) \\
& = 2\,V_c \sum_{n=1}^{\infty} J_{2n-1}(\frac{\omega_\Delta}{\omega_L})\,[\frac{1}{2} cos((\omega_c - (2n-1)\,\omega_L)\,t) - \frac{1}{2} cos((\omega_c + (2n-1)\,\omega_L)\,t)] \\
& = V_c \sum_{n=1}^{\infty} J_{2n-1}(\frac{\omega_\Delta}{\omega_L})\,[cos((\omega_c - (2n-1)\,\omega_L)\,t) - cos((\omega_c + (2n-1)\,\omega_L)\,t)]
\end{aligned}
\tag{B.6}
$$

Injecting those results back into equation (B.4) :

$$
\begin{aligned}
V(t) &= V_c\, J_0(\frac{\omega_\Delta}{\omega_L})\, cos(\omega_c t) + V_c \sum_{n=1}^{\infty} J_{2n}(\frac{\omega_\Delta}{\omega_L})\,[cos((\omega_c + 2n\,\omega_L)\,t) + cos((\omega_c - 2n\,\omega_L)\,t)] \\
&\quad + V_c \sum_{n=1}^{\infty} J_{2n-1}(\frac{\omega_\Delta}{\omega_L})\,[cos((\omega_c + (2n-1)\,\omega_L)\,t) - cos((\omega_c - (2n-1)\,\omega_L)\,t)] \\
&= V_c\, J_0(\frac{\omega_\Delta}{\omega_L})\, cos(\omega_c t) + V_c \sum_{n=1}^{\infty} J_n(\frac{\omega_\Delta}{\omega_L})\,[cos((\omega_c + n\,\omega_L)\,t) + (-1)^n\, cos((\omega_c - n\,\omega_L)\,t)]
\end{aligned}
\tag{B.7}
$$

Derivation of the expression for the square of $V(t)$, with the expression from equation (B.7) :

$$
\begin{aligned}
(V(t))^2 &= V_c^2\, J_0^2(\frac{\omega_\Delta}{\omega_L})\, cos^2(\omega_c t) \\
&\quad + 2\, V_c^2\, J_0(\frac{\omega_\Delta}{\omega_L})\, cos(\omega_c\, t) \sum_{n=1}^{\infty} J_n(\frac{\omega_\Delta}{\omega_L})\, [cos((\omega_c + n\,\omega_L)\, t) + (-1)^n\, cos((\omega_c - n\,\omega_L)\, t)] \\
&\quad + V_c^2 \sum_{n=1}^{\infty} J_n^2(\frac{\omega_\Delta}{\omega_L})\, [cos((\omega_c + n\,\omega_L)\, t) + (-1)^n\, cos((\omega_c - n\,\omega_L)\, t)]^2 \\
&= V_c^2\, J_0^2(\frac{\omega_\Delta}{\omega_L})\, cos^2(\omega_c t) \\
&\quad + 2\, V_c^2\, J_0(\frac{\omega_\Delta}{\omega_L}) \sum_{n=1}^{\infty} J_n(\frac{\omega_\Delta}{\omega_L})\, [cos(\omega_c\, t)\, cos((\omega_c + n\,\omega_L)\, t) + (-1)^n\, cos(\omega_c\, t)\, cos((\omega_c - n\,\omega_L)\, t)] \\
&\quad + V_c^2 \sum_{n=1}^{\infty} J_n^2(\frac{\omega_\Delta}{\omega_L})\, [cos^2((\omega_c + n\,\omega_L)\, t) \\
&\quad + 2\, cos((\omega_c + n\,\omega_L)\, t)\, (-1)^n\, cos((\omega_c - n\,\omega_L)\, t) + (-1)^{2n}\, cos^2((\omega_c - n\,\omega_L)\, t)] \\
&= V_c^2\, J_0^2(\frac{\omega_\Delta}{\omega_L})\, (\frac{1}{2} + \frac{1}{2}\, cos(2\,\omega_c\, t)) \\
&\quad + 2\, V_c^2\, J_0(\frac{\omega_\Delta}{\omega_L}) \sum_{n=1}^{\infty} J_n(\frac{\omega_\Delta}{\omega_L})[\frac{1}{2}\, cos((2\,\omega_c + n\,\omega_L)\, t) + \frac{1}{2}\, cos(n\,\omega_L\, t) \\
&\quad + \frac{1}{2}\, (-1)^n\, cos((2\,\omega_c - n\,\omega_L)\, t) + \frac{1}{2}\, (-1)^n\, cos(n\,\omega_L\, t)] \\
&\quad + V_c^2 \sum_{n=1}^{\infty} J_n^2(\frac{\omega_\Delta}{\omega_L})\, [\frac{1}{2} + \frac{1}{2}\, cos((2\,\omega_c + 2n\,\omega_L)\, t) \\
&\quad + 2\, (-1)^n\, (\frac{1}{2}\, cos(2\,\omega_c\, t) + \frac{1}{2}\, cos(2n\,\omega_L\, t)) + \frac{1}{2} + \frac{1}{2}\, cos((2\,\omega_c - 2n\,\omega_L)\, t)] \\
&= \frac{1}{2}\, V_c^2\, J_0^2(\frac{\omega_\Delta}{\omega_L})\, (1 + cos(2\,\omega_c\, t)) \\
&\quad + V_c^2\, J_0(\frac{\omega_\Delta}{\omega_L}) \sum_{n=1}^{\infty} J_n(\frac{\omega_\Delta}{\omega_L})[cos((2\,\omega_c + n\,\omega_L)\, t) + (-1)^n\, \underbrace{cos((2\,\omega_c - n\,\omega_L)\, t)}_{\text{C}} \\
&\quad + 2\, V_c^2\, J_0(\frac{\omega_\Delta}{\omega_L}) \sum_{n=1}^{\infty} cos(2n\,\omega_L\, t) + V_c^2 \sum_{n=1}^{\infty} J_n^2(\frac{\omega_\Delta}{\omega_L})\, [1 + \frac{1}{2}\, cos((2\,\omega_c + 2n\,\omega_L)\, t) \\
&\quad + (-1)^n\, (cos(2\,\omega_c\, t) + cos(2n\,\omega_L\, t)) + \frac{1}{2}\, \underbrace{cos((2\,\omega_c - 2n\,\omega_L)\, t)]}_{\text{D}} \qquad \text{(B.8)}
\end{aligned}
$$

It is straightforward to see that the only terms that could be at the frequency ω_L are the parts C and D highlighted in equation (B.8). We can then easily choose suitable values for ω_c and ω_L so that the frequency is not present in the development.

Derivation : mechanical displacement $\delta x(t + \Delta t)$

The equation of motion of a damped oscillator is :

$$m\,\ddot{x}(t) + \frac{m\,\omega_0}{Q}\,\dot{x}(t) + m\,\omega_0^2\,x(t) = F(t) \tag{B.9}$$

The force on the nanotube is expressed as :

$$\begin{aligned} F(t) = \frac{1}{2}\,C'\,V^2(t) &= \frac{C'}{2}\,(V_g^{DC} - V_{offset} - V^{FM}(t))^2 \\ &= \underbrace{(V_g^{DC})^2 + V_{offset}^2 - 2V_g^{DC}\,V_{offset}}_{\text{DC}} + \underbrace{(V^{FM}(t))^2}_{\substack{\text{high frequencies} \\ \text{no motion}}} \\ &\quad - 2\,(V_g^{DC} - V_{offset})\,V^{FM}(t) \end{aligned} \tag{B.10}$$

From equation (B.10), we see that the force has different components : some at constant voltage, which are only applying stresses on the nanotube, others at high frequencies, far from the peak of resonance and therefore without impact on the motion and finally components from $V^{FM}(t)$, close to the resonance frequency. In the following analysis, we only consider the terms responsible for the motion of the nanotube. Since the resonator cannot detect the modulation, it is assumed that the force is applied at a constant frequency ω_i during the time step of the oscillator. Therefore the frequency modulation signal becomes : $V^{FM}(t) = V_c\,cos(\omega_i\,\Delta t + \Psi(t))$. That assumption greatly simplifies the following analysis.
From the equation of motion :

$$m\,\ddot{x}(t) + \frac{m\,\omega_0}{Q}\,\dot{x}(t) + m\,\omega_0^2\,x(t) = -C'\,(V_g^{DC} - V_{offset})\,V_c\,cos(\omega_i\,\Delta t + \Psi(t)) \tag{B.11}$$

Applying the Fourier Transform :

$$-\,m\,\omega^2\,X(\omega) - i\frac{m\,\omega\,\omega_0}{Q}\,X(\omega) + m\,\omega_0^2\,X(\omega) = -C'\,(V_g^{DC} - V_{offset})\,V_c\,\delta(\omega - \omega_i) \tag{B.12}$$

Finally :

$$\begin{aligned} X(\omega) &= \frac{-C'\,(V_g^{DC} - V_{offset})}{m}\,\frac{V_c}{\omega_0^2 - \omega^2 - i\,\frac{\omega\,\omega_0}{Q}}\,\delta(\omega - \omega_i) \\ &= \delta x*(\omega)\,\delta(\omega - \omega_i) \\ &= \delta x*(\omega_i) \end{aligned} \tag{B.13}$$

The instantaneous mechanical displacement of the nanotube is given by the real

part of the inverse Fourier Transform :

$$\begin{aligned}\delta x(t+\Delta t) &= \mathrm{Re}\{\int_{-\infty}^{\infty} X(\omega)\, e^{i\,\omega\, t} d\,\omega\} = \mathrm{Re}\{\int_{-\infty}^{\infty} \delta x*(\omega_i)\, e^{i\,\omega\, t} d\,\omega\} \\ &= \mathrm{Re}\{\delta x*(\omega_i)\, e^{i\,\omega_i\, t}\} \\ &= \mathrm{Re}\{\delta x*(\omega_i)\,(cos(\omega_i\,\Delta t+\Psi(t))+i\,sin(\omega_i\,\Delta t+\Psi(t))\} \\ &= \mathrm{Re}\{\delta x*(\omega_i)\}\,cos(\omega_i\,\Delta t+\Psi(t)) - \mathrm{Im}\{\delta x*(\omega_i)\}\,sin(\omega_i\,\Delta t+\Psi(t))\end{aligned} \tag{B.14}$$

Verification of the results obtained

The following variables are defined : $\omega_0/2\pi = 10^6$, $Q = 1000$. The Lorentzian is the frequency response of the motion. In our case, after normalization, we get :

$$\delta x(\omega) = \frac{1}{\omega_0^2 - \omega^2 + j\,\frac{\omega_0\,\omega_i}{Q}} \approx \frac{1}{2\,\omega_0(\omega_0-\omega) + j\,\frac{\omega_0^2}{Q}} \tag{B.15}$$

The real part of the Lorentzian is

$$\mathrm{Re}\{\delta x(\omega)\} = -\frac{-2\omega_0\,(\omega_0-\omega)\,Q^2}{\omega_0^2\,(4Q^2\,(\omega-\omega_0)^2+\omega_0^2)} \tag{B.16}$$

and its first derivative

$$\frac{\partial \mathrm{Re}\{\delta x(\omega)\}}{\partial\omega} = \frac{8Q^4\,(\omega-\omega_0)^2 - 2Q^2\,\omega_0^2}{\omega_0\,(4Q^2\,(\omega-\omega_0)^2+\omega_0^2)^2} \tag{B.17}$$

Figure 17 shows the derivative of the real part of the Lorentzian. It qualitatively matches the results obtained in [17].

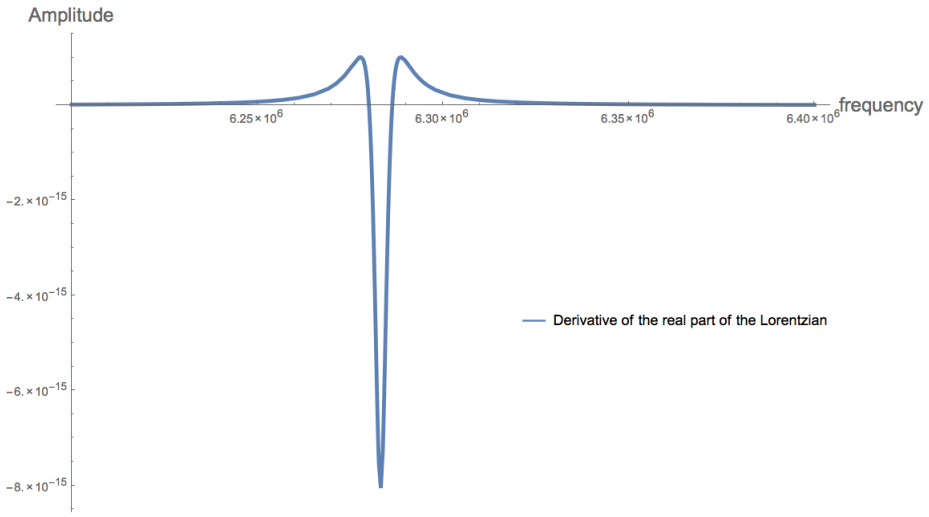

Figure 17: Derivative of the real part of the Lorentzian